Am J Cancer Res 2026;16(1):51-69
www.ajcr.us /ISSN:2156-6976/ajcr0169142

Original Article

CCT5 as a candidate biomarker in bladder cancer: functional validation and mechanistic clues

Xiaojun Zhang[1,2], Yuqiang Fu[1,2], Yuelin Du[1,2], Wei Xiong[1,2], Jieneng Wang[3], Helin Zhang[1,2], Yao Luo[1,2], Yanzong Zhao[4*], Panfeng Shang[1,2*]

[1]Department of Urology, Gansu Province Clinical Research Center for Urinary System Disease, The Second Hospital of Lanzhou University, Lanzhou 730030, Gansu, China; [2]Institute of Urology, Gansu Province Clinical Research Center for Urinary System Disease, The Second Hospital of Lanzhou University, Lanzhou 730030, Gansu, China; [3]Department of Cardiovascular, The First Hospital of Lanzhou University, Lanzhou 730000, Gansu, China; [4]Department of Urology, The First Hospital of Lanzhou University, Lanzhou 730000, Gansu, China. [*]Co-corresponding authors.

Received October 5, 2025; Accepted January 4, 2026; Epub January 15, 2026; Published January 30, 2026

Abstract: CCT5, a subunit of the chaperonin-containing TCP1 complex, has been implicated in the development of various malignancies. However, its role in bladder cancer remains undefined. This study investigated the functional contribution of CCT5 and its association with Hippo/YAP signaling. Using data from The Cancer Genome Atlas (TCGA) and Gene Expression Omnibus (GEO), CCT5 expression and its prognostic significance were analyzed. Single-cell and spatial transcriptomics were employed to explore expression patterns and cellular heterogeneity. Functional assessments were conducted *in vitro* and *in vivo* using xenografts. To elucidate the underlying mechanisms, RNA-seq was integrated with Western blotting analysis. CCT5 was found to be upregulated in bladder cancer and correlated with poor prognosis and aggressive pathological features. Single-cell and spatial analyses revealed that CCT5 was enriched in malignant epithelial subpopulations with high CNV scores, activated oncogenic pathways, and extensive cell-cell interactions. Functionally, CCT5 promoted proliferation, migration, invasion, and G1/S transition while inhibiting apoptosis; its depletion reduced xenograft growth. At the signaling level, CCT5 knockdown enhanced phosphorylation of MST1, LATS1, and YAP, without significant changes in total protein levels, suggesting activation of Hippo/YAP signaling. These findings highlight CCT5 as an oncogenic factor in bladder cancer, potentially acting through the regulation of Hippo/YAP signaling, and propose its potential as a biomarker and therapeutic target in bladder cancer.

Keywords: CCT5, bladder cancer, Hippo/YAP signaling, cell cycle, apoptosis

Introduction

Bladder cancer (BLCA), with a high incidence among urological diseases, remains one of the ten most prevalent cancers globally. According to GLOBOCAN 2022, approximately 613,791 new cases and 220,349 deaths were reported, emphasizing its significant disease burden [1]. While cystoscopy remains the diagnostic gold standard, certain lesions can still be missed [2]. Although molecular markers such as TP53, ERCC1, and FGFR3 have been explored for diagnostic and therapeutic applications, their practical utility remains limited, making early detection a continuing challenge [3, 4]. Despite advancements in surgical approaches, systemic treatments, and immunotherapies, patient outcomes remain suboptimal, primarily due to high recurrence rates, aggressive progression, and therapy resistance [5-7]. Therefore, there is an urgent need for sensitive biomarkers and precise therapeutic targets in BLCA.

The chaperonin-containing TCP-1 (CCT), also known as the TRiC complex, is a type II molecular chaperonin specific to eukaryotes. Composed of eight distinct subunits, it assists in the proper folding of a variety of substrates, including STAT3, the von Hippel-Lindau (VHL) tumor suppressor, actin, tubulin, and cell cycle regulators [8-12]. These substrates are critical for tumor-related processes such as proliferation, invasion, and migration. Among the CCT subunits, CCT5 has been found to be upregulated

in several cancers, correlating with malignant features and poor clinical outcomes, suggesting an oncogenic role [13-20]. However, the specific function and mechanistic basis of CCT5 in BLCA remain unclear.

The Hippo signaling pathway is a vital regulatory network that controls organ development, cell proliferation, immune response, and tissue homeostasis [21]. It operates through a kinase cascade, involving MST1/2, LATS1/2, YAP, and TAZ [22]. Upon activation, MST1/2 are phosphorylated, which in turn activates LATS1/2 phosphorylation. This cascade leads to YAP phosphorylation, resulting in its sequestration in the cytoplasm and inhibition of transcriptional activity [22-24]. In BLCA, the Hippo pathway plays a key role in disease progression, poor prognosis, and immune evasion [25, 26]. Therefore, exploring whether CCT5 influences BLCA progression by modulating the Hippo pathway is of significant research interest.

This study comprehensively examined CCT5 expression, its prognostic relevance, and its functional roles in BLCA by integrating TCGA and GEO datasets with clinical tissue samples. These findings were further validated through experiments in both cultured cells and animal models. Our results show that CCT5 expression is elevated in BLCA tissues and associated cancer cells, with higher expression linked to poor prognosis and more aggressive pathological features. Functional analyses revealed that CCT5 promotes proliferation, migration, invasion, and G1/S phase progression while inhibiting apoptosis in BLCA cells. Mechanistically, CCT5 accelerates BLCA progression by modulating the Hippo/YAP signaling pathway. In summary, our findings highlight CCT5 as an oncogenic driver in BLCA, suggesting its potential as both a diagnostic marker and a therapeutic target.

Materials and methods

CCT5 expression and functional analysis

The TCGA dataset for BLCA (https://cancergenome.nih.gov) was utilized to assess CCT5 expression, its prognostic significance, and potential biological relevance. For differential expression analysis, tumor samples were ranked by CCT5 expression and stratified using the median value as a cutoff, dividing the samples into CCT5-low (bottom 50%) and CCT5-high (top 50%) groups. Differential expression was analyzed using DESeq2 in R 4.2.1 ($|\log_2 FC| > 1$; FDR < 0.05, Benjamini-Hochberg), and graphics were generated with ggplot2. Survival analyses were performed using Kaplan-Meier curves and log-rank testing *via* the survival R package. To explore functional associations, genes correlated with CCT5 were analyzed for Gene Ontology (GO) terms, Kyoto Encyclopedia of Genes and Genomes (KEGG) pathways, and gene set enrichment analysis (GSEA) using the clusterProfiler R package. For improved reliability of co-expression-based enrichment, CCT5 co-expressed genes were defined with a correlation threshold ($|R| > 0.6$ and FDR < 0.05), and the resulting gene set was used for downstream GO/KEGG enrichment analyses. Receiver operating characteristic (ROC) curves were computed using the pROC package. Associations between CCT5, immune infiltration, and immune checkpoints were explored with ssGSEA. Validation of CCT5 expression differences was performed using GEO datasets GSE7476 and GSE13507 (https://www.ncbi.nlm.nih.gov/geo).

Single-cell RNA-sequencing analysis

Single-cell RNA sequencing (scRNA-seq) data for BLCA were retrieved from the GEO database (GSE135337), which served as the primary resource for cell-type annotation, epithelial subclustering (CCT5-high/CCT5-low), inferCNV analysis, differential expression-based enrichment, and cell-cell communication analysis. Additionally, an independent scRNA-seq dataset (GSE145137) was used to validate the cell-type-specific expression of CCT5. Spatial transcriptomics analysis was conducted *via* the CNGB STOmics platform (https://db.cngb.org/stomics/) to visualize the spatial distribution of CCT5 expression in BLCA tissues. Doublet scores were calculated using Scrublet, and cells were filtered based on the following criteria: doublet score < 0.3, mitochondrial gene proportion < 10%, detected genes 500-7000, and counts 1000-40,000. After quality control, 21,767 high-quality cells were retained. Data were preprocessed using Scanpy (v1.9.1), including normalization and identification of highly variable genes. Dimensionality reduction was performed by PCA, batch effects were corrected using Harmony, and unsupervised clustering

was carried out using the Leiden algorithm to construct a k-nearest neighbor graph. UMAP was used for visualization. Cell types were annotated based on canonical marker genes, including epithelial cells (EPCAM, KRT19), T lymphocytes (CD3D, CD3E), and B lymphocytes (CD79A, MS4A1). CCT5 expression was visualized at single-cell resolution using FeaturePlot; epithelial subsets with higher overall CCT5 expression were labeled as Epithelial_CCT5_high, and others were labeled as Epithelial_CCT5_low. During atlas construction, epithelial cells from benign BCN samples were retained, and sample-of-origin mapping was performed to assess the distribution of epithelial states between BC and BCN samples. Copy number variations (CNVs) were inferred using inferCNV (v1.6.0), with epithelial cells as observations and T cells from all samples as the reference population to establish a diploid baseline for CNV inference across the integrated dataset. Intercellular communication networks were analyzed using CellChat (v1.1.3) to identify ligand-receptor interactions between Epithelial_CCT5_high cells and other annotated cell types.

Cell lines and human tissue specimens

The Institute of Urological Diseases at the Second Hospital of Lanzhou University (Lanzhou, China) provided the normal human urothelial cell line SV-HUC-1 and BLCA cell lines (UMUC-3, T24, J82, 253J, and 5637). The cell lines were cultured in either Ham's F-12K (Gibco) or RPMI-1640 (Shanghai Yuanpei), with both media supplemented with 1% streptomycin, 1% penicillin, and 10% fetal bovine serum (FBS).

BLCA tissue specimens were collected from the Department of Urology, Second Hospital of Lanzhou University, with approval from the institutional ethics committee (Approval No. 2025A-517) and written informed consent obtained from each participant.

Immunohistochemistry (IHC)

IHC was performed using the UltraSensitive™ SP kit (Maixin Biotechnology, KIT-9710) according to the manufacturer's protocol. Briefly, tissue sections were baked, deparaffinized, rehydrated through graded alcohols, and subjected to antigen retrieval in EDTA buffer, followed by cooling and PBS washing. Endogenous peroxidase activity and nonspecific binding were blocked using reagents from the kit. Sections were incubated overnight at 4°C with primary antibodies against CCT5 (1:200, Proteintech, 11603-1-AP) and Ki67 (1:1000, Proteintech, 27309-1-AP). After returning to room temperature, biotin-conjugated goat anti-mouse/rabbit IgG polymer and streptavidin peroxidase were applied sequentially. Immunostaining was visualized using 3,3'-diaminobenzidine (DAB; Maixin Biotechnology, KIT-0015), followed by hematoxylin counterstaining, ethanol dehydration, and mounting with neutral resin.

Quantitative real-time polymerase chain reaction (RT-qPCR)

Total RNA was extracted using the Steady-Pure RNA Extraction Kit (Accurate Biotechnology, AG21023) following the product manual. RNA extraction efficiency was assessed using a NanoDrop 2000, and reverse transcription was performed according to the kit protocol (Accurate Biotechnology, AG11728). RT-qPCR was conducted following the manufacturer's instructions (Accurate Biotechnology, AG11701). The reaction began with 95°C for 30 seconds (denaturation), followed by 40 cycles of 95°C for 5 seconds and 60°C for 30 seconds. CCT5 levels were calculated as $2^{-\Delta\Delta Ct}$ values and normalized to β-actin [27]. Each reaction was performed in triplicate to ensure reproducibility. Primer sequences are provided in Table S1.

Protein extraction and Western blotting

As previously reported [28], total cellular proteins were extracted. Samples were separated using a 10% SDS-PAGE system and transferred to PVDF membranes. Blocking was performed with TBST containing 5% non-fat milk at 37°C for 90 minutes. The membranes were then incubated with diluted primary antibodies at 4°C overnight. After treatment with secondary antibodies for 1 hour, protein signals were visualized and analyzed using a dual-infrared imaging system. The following antibodies were used: GAPDH (1:1000; Servicebio, #GB15004-100), CCT5 (1:1000; Proteintech, #11603-1-AP), CDK4 (1:1000; Proteintech, #11026-1-AP), CDK6 (1:1000; Proteintech, #14052-1-AP), Cyclin D1 (1:1000; Proteintech, #26939-1-AP), phospho-MST1/2 (1:1000; Cell Signaling Technology, #49332), MST1 (1:500; Santa Cruz, #sc-

515051), LATS1 (1:500; Santa Cruz, #sc-398560), phospho-LATS1 (1:1000; Cell Signaling Technology, #8654), YAP1 (1:500; Santa Cruz, #sc-101199), and phospho-YAP1 (1:1000; Abways, #CY5743).

Cell transfection

CCT5 knockdown and overexpression plasmids were synthesized by Miaolingbio (Wuhan, China). UMUC-3, T24, and J82 cells were transfected using polyethylenimine (PEI; Servicebio, G1802-1ML) following the manufacturer's protocol. Stable transfectants were generated through puromycin selection. The efficiency of knockdown and overexpression was assessed using RT-qPCR and Western blotting analysis. Relevant sequences are provided in Table S2. In the CCT5 knockdown validation experiment, cells were divided into three groups: negative control (NC), CCT5 knockdown (Sh1), and CCT5 knockdown (Sh2). For the CCT5 overexpression validation experiment, the groups were: negative control (Vector) and CCT5 overexpression (OE).

Cell proliferation assay

The proliferation assay was conducted in 96-well plates, with approximately 2,000 cells seeded per well. Reagents were added according to the manufacturer's instructions on days 0, 1, 2, 3, and 4 after cell attachment, and absorbance was measured at 450 nm. All assays were performed in triplicate. Data analysis and visualization were done using GraphPad Prism 10.

Cell colony assay

For the clonogenic assay, approximately 1,000 cells were seeded per well in six-well culture dishes and cultured for two weeks under appropriate conditions. The medium was then removed, and colonies were fixed with 4% paraformaldehyde for 30 minutes, stained with diluted crystal violet, and counted using a microscope. All assays were performed in triplicate to ensure reproducibility.

Scratch assay

For the scratch assay, when cell density reached approximately 80%, a uniform scratch was made using a pipette tip perpendicular to the dish surface. After washing with PBS, the initial gap width (0 h) was recorded using microscopy. Cells were cultured for an additional 24 hours, after which the gap closure was re-evaluated by imaging.

Transwell assays

In the migration assay, 600 μL of complete medium was added to the bottom wells, and 200 μL of serum-free cell suspension (20,000 cells) was seeded into the insert. Cells were incubated for 24 hours.

For the invasion assay, 600 μL of medium (10% FBS) was added to the bottom wells. Matrigel was diluted to one-ninth of its original concentration and applied to the upper surface of the chamber. Then, 200 μL of serum-free cell suspension (20,000 cells) was added, and cells were cultured for 2 days.

After fixation (paraformaldehyde) and staining (crystal violet), five random fields per chamber were captured and analyzed using ImageJ.

Cell cycle and apoptosis assays

For the cell cycle assay, cells at approximately 80% confluence were processed using the Cell Cycle Assay Kit (Linkebio, CCS012) according to the kit protocol and analyzed *via* flow cytometry. A total of 1×10^6 cells were collected, prepared as per the instructions of the corresponding kit (Linkebio, AP101), and analyzed.

Xenograft tumor model

The nude mice were obtained from the Experimental Animal Center of the Lanzhou Veterinary Research Institute, Chinese Academy of Agricultural Sciences. Fifteen 5-week-old female nude mice (weighing between 18 and 20 g) were maintained in specific pathogen-free (SPF) conditions, with access to autoclaved chow and sterilized water ad libitum. The mice were randomly assigned to three groups (five mice per group): NC, CCT5 knockdown (Sh1), and CCT5 knockdown (Sh2). UMUC-3 cells were resuspended in Matrigel mixed with physiological saline at a 1:1 ratio, and 1×10^6 cells were subcutaneously injected into each mouse. Tumor growth was monitored every 3 days using calipers. Mice were closely observed throughout the experiment, with humane end-

points predefined. Upon reaching the ethical tumor volume endpoint of approximately 1000 mm^3, mice were euthanized by cervical dislocation, and tumors were harvested for imaging, weighing, and fixation. Tumor volume was calculated using the formula V = (length × $width^2$)/2. The Experimental Animal Welfare and Ethics Committee of the Second Hospital of Lanzhou University approved all animal studies (Approval No. D2025-412), which were conducted in accordance with institutional guidelines.

RNA sequencing

Following the manufacturer's protocol, sufficient quantities of control and CCT5-knockdown T24 cells were collected and snap-frozen in liquid nitrogen for temporary storage. RNA sequencing and primary data processing were performed by Guoke Andes Biotechnology Co., Ltd. (Hangzhou, China). Differentially expressed genes were identified using a threshold of $|\log_2 FC| > 1$ and an adjusted *p*-value (padj) < 0.05, followed by functional enrichment analysis.

Statistical analysis

Summary statistics (mean ± SD; n = 3) were calculated using GraphPad Prism (v10.0). Student's t-test was used for pairwise (two-group) comparisons, while one-way ANOVA with Tukey's post hoc test was applied for comparisons involving more than two groups. Statistical significance was defined as $P < 0.05$, with results above this threshold considered non-significant (ns). All experiments were independently repeated three times. Computational analyses of bulk and single-cell transcriptomes, as well as figure generation, were performed using R (v4.2.1) and Python (v3.10), with commonly used packages such as ggplot2, pheatmap, Seurat, and Scanpy.

Result

The expression level of CCT5 was significantly increased in bladder cancer

Pan-cancer analysis revealed a significant upregulation of CCT5 expression across 17 tumor types, including BLCA (**Figure 1A**, **1B**). Further examination of BLCA data showed consistently higher CCT5 levels in tumor tissues compared to adjacent normal tissues, both in paired and unpaired cohorts (**Figure 1C**, **1D**). This finding was confirmed by results from two external GEO datasets, GSE7476 and GSE13507 (**Figure 1E**, **1F**). IHC staining further supported these observations, showing markedly stronger CCT5 staining in patient-derived BLCA specimens than in normal urothelial controls (**Figure 1G**). Consistent with these results, RT-qPCR analysis of clinical samples demonstrated significantly higher CCT5 mRNA levels in tumors compared to paired adjacent noncancerous tissues (**Figure 1H**). Additionally, CCT5 expression was notably elevated in BLCA cell lines (UMUC-3, 5637, J82, T24, and 253J) at both the transcript and protein levels, as confirmed by RT-qPCR and Western blotting analysis, compared to the normal urothelial line SV-HUC-1 (**Figure 1I**, **1J**).

High CCT5 expression correlates with poor survival and aggressive clinical features in bladder cancer

Kaplan-Meier survival curves indicated that patients with high CCT5 expression had significantly poorer overall survival (OS), disease-specific survival (DSS), and progression-free survival (PFS) compared to the low-expression group (**Figure 2A-C**). CCT5 expression was significantly higher in T2-T4 tumors and pathological stage II-IV compared to normal tissues, but no consistent stepwise increase in expression across advanced stages was observed (**Figure 2D**, **2E**). Furthermore, CCT5 levels were markedly higher in non-papillary subtypes compared to papillary subtypes and in high-grade tumors relative to low-grade tumors (**Figure 2F**, **2G**). ROC curve analysis demonstrated that CCT5 had strong diagnostic potential for distinguishing BLCA tissues from adjacent normal tissues, with an AUC of 0.835 (**Figure 2H**).

Enrichment analysis of CCT5 in bladder cancer

To further investigate the role of CCT5 in BLCA, this study identified 2,176 genes that were differentially expressed between the CCT5-high and CCT5-low groups (**Figure 3A**) and 746 genes significantly correlated with CCT5 expression. A heatmap displaying the top 20 genes positively correlated with CCT5 is shown in **Figure 3B**. GO enrichment analysis revealed that these co-expressed genes were primarily associated with cell cycle-related processes,

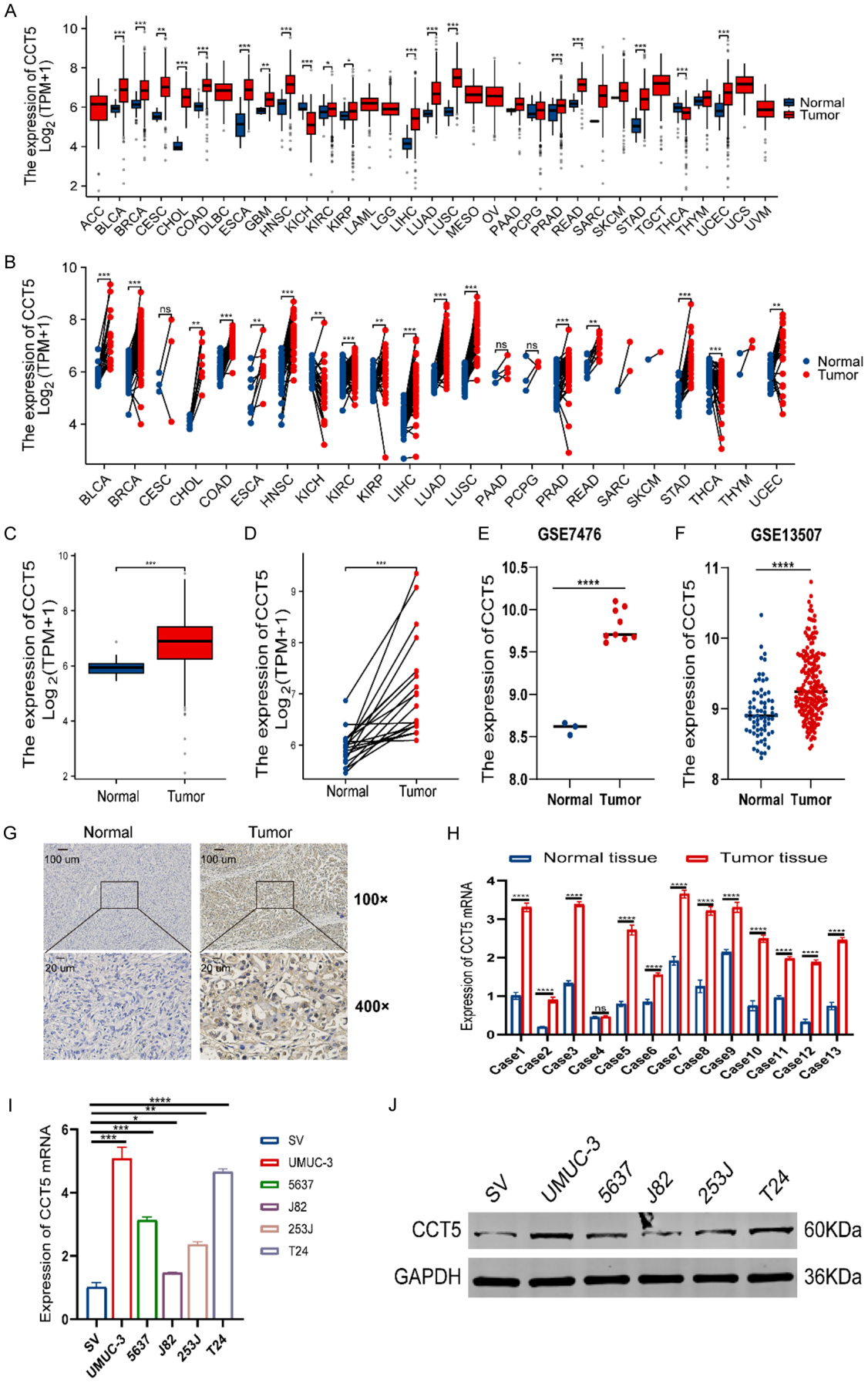
A
The expression of CCT5 Log2 (TPM+1)
Normal
Tumor
ACC BLCA BRCA CESC CHOL COAD DLBC ESCA GBM HNSC KICH KIRC KIRP LAML LGG LIHC LUAD LUSC MESO OV PAAD PCPG PRAD READ SARC SKCM STAD TGCT THCA THYM UCEC UCS UVM
B
The expression of CCT5 Log2 (TPM+1)
Normal
Tumor
BLCA BRCA CESC CHOL COAD ESCA HNSC KICH KIRC KIRP LIHC LUAD LUSC PAAD PCPG PRAD READ SARC SKCM STAD THCA THYM UCEC
C
The expression of CCT5 Log2(TPM+1)
Normal Tumor
D
The expression of CCT5 Log2(TPM+1)
Normal Tumor
E
GSE7476
The expression of CCT5
Normal Tumor
F
GSE13507
The expression of CCT5
Normal Tumor
G
Normal
Tumor
100 um
20 um
100×
400×
H
Normal tissue
Tumor tissue
Expression of CCT5 mRNA
Case1 Case2 Case3 Case4 Case5 Case6 Case7 Case8 Case9 Case10 Case11 Case12 Case13
I
Expression of CCT5 mRNA
SV
UMUC-3
5637
J82
253J
T24
J
SV UMUC-3 5637 J82 253J T24
CCT5
GAPDH
60KDa
36KDa

Figure 1. Upregulation of CCT5 was observed in bladder cancer. A, B. Pan-cancer analysis of CCT5 expression across 33 tumor types from the TCGA database. C, D. Evaluation of CCT5 expression in paired and unpaired samples from TCGA-BLCA cohorts. E, F. Validation of elevated CCT5 expression in BLCA using GSE7476 and GSE13507. G. Immunohistochemical staining of clinical specimens reveals stronger CCT5 expression in bladder tumor tissues compared to normal urothelium. H. RT-qPCR results demonstrating upregulation of CCT5 in bladder carcinoma tissues relative to matched adjacent non-cancerous tissues. I, J. RT-qPCR and Western blot analyses confirm higher CCT5 levels in UMUC-3, 5637, J82, T24, and 253J than in the SV-HUC-1.

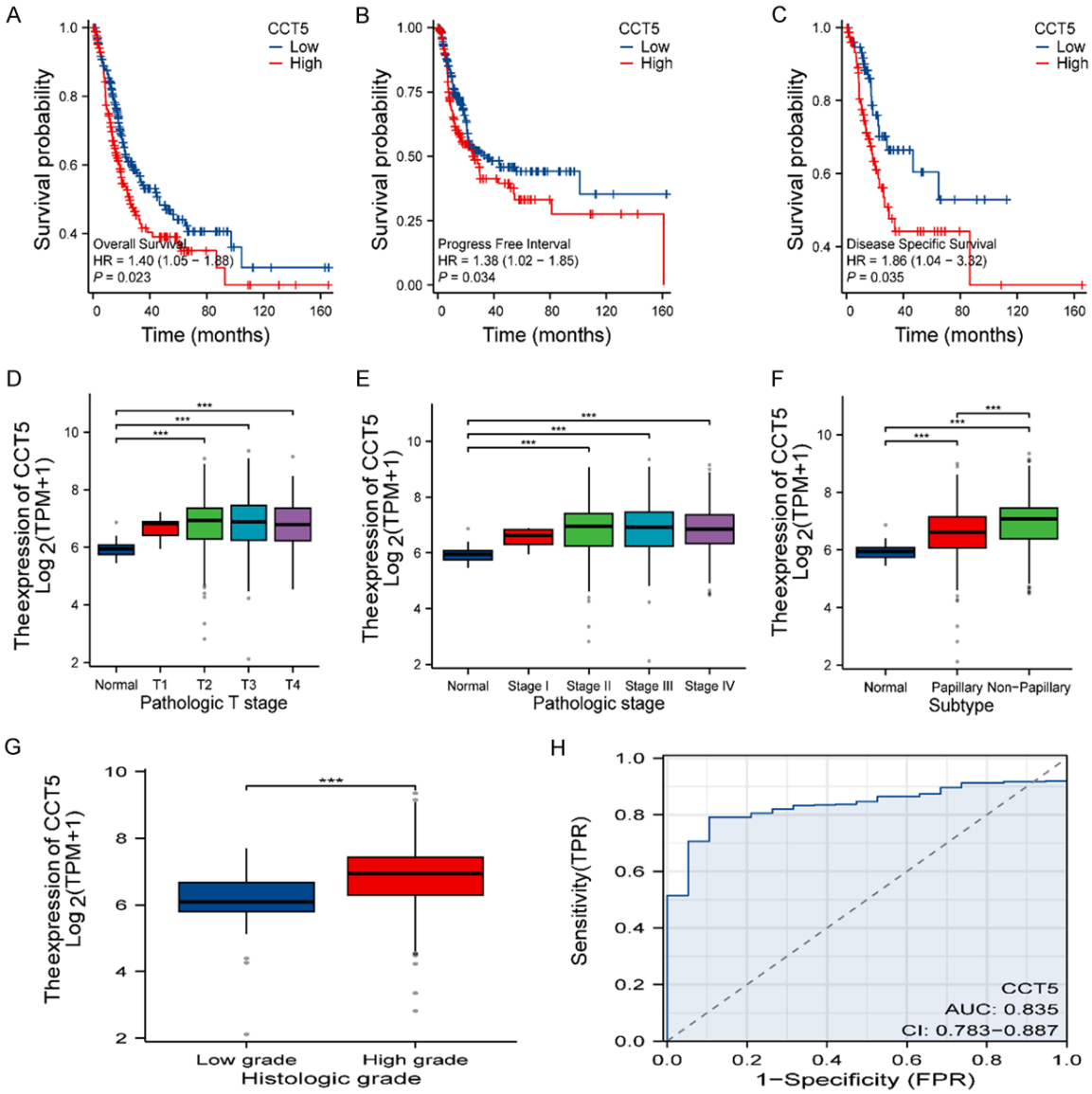

Figure 2. High CCT5 expression correlates with poor survival and aggressive clinical features. A-C. Kaplan-Meier curves revealed that high CCT5 expression was correlated with adverse survival outcomes. D, E. Differential expression of CCT5 across distinct stages of BLCA. F, G. Expression variations of CCT5 between papillary and non-papillary subtypes, as well as between low-grade and high-grade BLCA. H. ROC analysis underscored the strong diagnostic capacity of CCT5 (AUC = 0.835).

including DNA replication, mitotic phase transition, and regulation of DNA metabolism (**Figure 3C**). Additionally, these genes were enriched in chromosomal regions, spindle structures, and microtubule assemblies (**Figure 3D**). Molecular function analysis revealed significant enrichment in ATP hydrolysis activity, tubulin binding, GTPase binding, and chaperone-mediated pro-

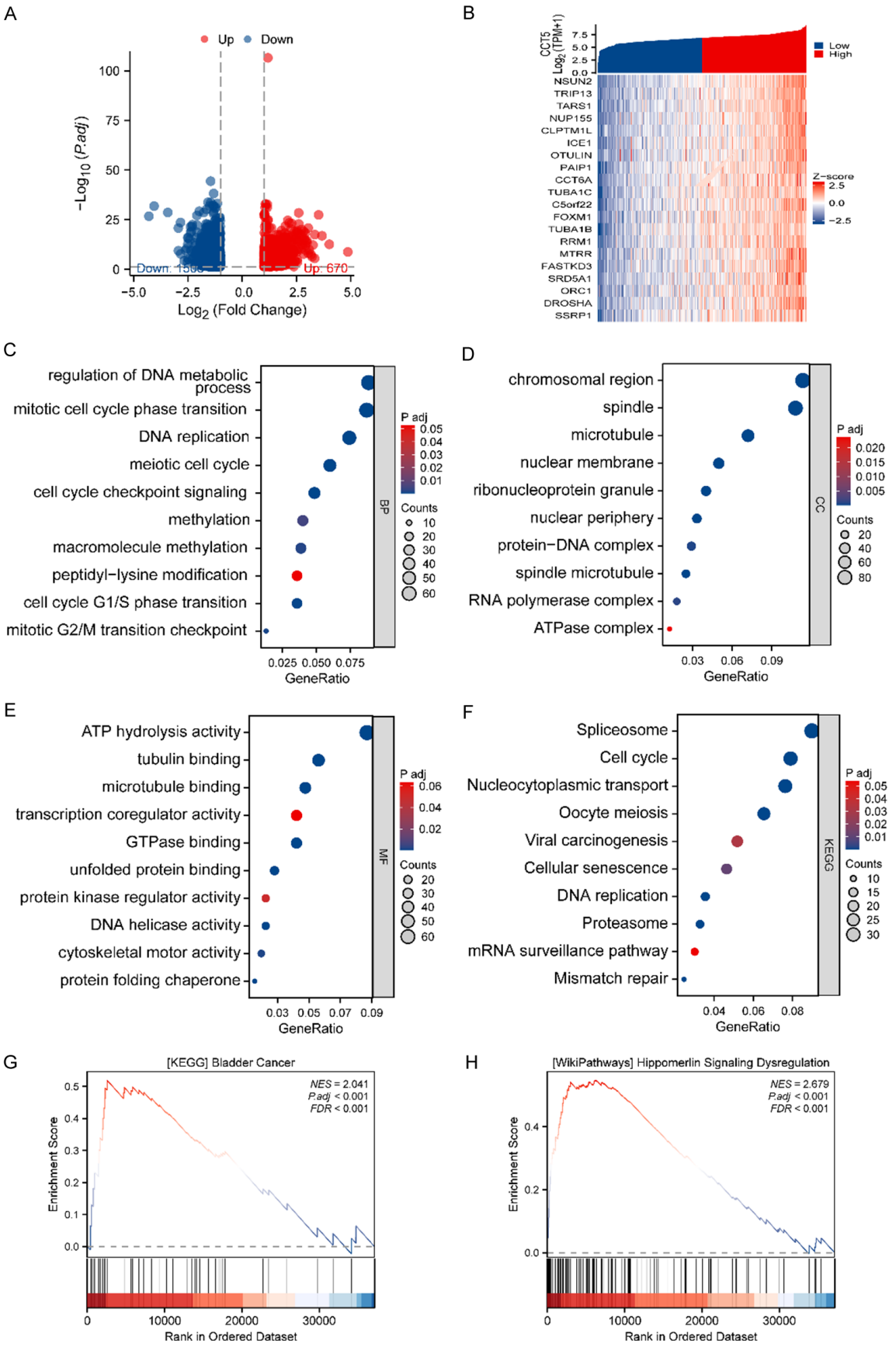
A
Up
Down
−Log10 (P.adj)
Log2 (Fold Change)
Down: 1586
Up: 670
B
CCT5 Log2 (TPM+1)
Low
High
NSUN2
TRIP13
TARS1
NUP155
CLPTM1L
ICE1
OTULIN
PAIP1
CCT6A
TUBA1C
C5orf22
FOXM1
TUBA1B
RRM1
MTRR
FASTKD3
SRD5A1
ORC1
DROSHA
SSRP1
Z−score
C
regulation of DNA metabolic process
mitotic cell cycle phase transition
DNA replication
meiotic cell cycle
cell cycle checkpoint signaling
methylation
macromolecule methylation
peptidyl−lysine modification
cell cycle G1/S phase transition
mitotic G2/M transition checkpoint
BP
P adj
Counts
GeneRatio
D
chromosomal region
spindle
microtubule
nuclear membrane
ribonucleoprotein granule
nuclear periphery
protein−DNA complex
spindle microtubule
RNA polymerase complex
ATPase complex
CC
E
ATP hydrolysis activity
tubulin binding
microtubule binding
transcription coregulator activity
GTPase binding
unfolded protein binding
protein kinase regulator activity
DNA helicase activity
cytoskeletal motor activity
protein folding chaperone
MF
F
Spliceosome
Cell cycle
Nucleocytoplasmic transport
Oocyte meiosis
Viral carcinogenesis
Cellular senescence
DNA replication
Proteasome
mRNA surveillance pathway
Mismatch repair
KEGG
G
[KEGG] Bladder Cancer
NES = 2.041
P.adj < 0.001
FDR < 0.001
Enrichment Score
Rank in Ordered Dataset
H
[WikiPathways] Hippomerlin Signaling Dysregulation
NES = 2.679
P.adj < 0.001
FDR < 0.001

Figure 3. Functional enrichment analysis of CCT5-related genes in BLCA. A. Volcano plot of DEGs between the CCT5-high and CCT5-low groups in the TCGA-BLCA cohort. B. Heatmap of the top 20 positively correlated genes with CCT5 in the TCGA-BLCA cohort. C-E. GO enrichment analysis of CCT5-co-expressed genes in BP, CC, and MF. F. KEGG analysis showed enrichment in the cell cycle pathway. G, H. GSEA linked high CCT5 expression to dysregulation of bladder cancer and Hippo signaling pathways.

tein folding (**Figure 3E**). Pathway enrichment analysis identified key pathways associated with these genes, including the cell cycle, oocyte meiosis, and spliceosome (**Figure 3F**). Moreover, GSEA highlighted that elevated CCT5 expression was linked to dysregulation of BLCA-related pathways and the Hippo signaling pathway (**Figure 3G**, **3H**). These results suggest that CCT5 may act as an oncogenic driver in BLCA by promoting cell cycle progression and disrupting Hippo signaling.

Single-cell transcriptomic analysis reveals epithelial CCT5-high subclusters with increased malignancy

To comprehensively investigate the functional role of CCT5 in BLCA, scRNA-seq data from the GSE135337 cohort were analyzed. After rigorous quality assessment (Figure S1A-H), 21,767 high-quality cells meeting the quality thresholds were included for further analysis. UMAP projection and cell-type annotation identified major populations, including epithelial, immune, endothelial, and stromal cells (**Figure 4A**, **4B**). Marker gene dot plots confirmed these annotations: B cells were marked by CD79A/MS4A1, endothelial cells by PECAM1/VWF, epithelial cells by EPCAM/KRT19, fibroblasts by DCN/COL1A1, myeloid cells by AIF1/LYZ, and T cells by CD3D/CD3E (**Figure 4C**). The feature plot revealed that CCT5 expression was primarily detected in clusters annotated as epithelial cells (**Figure 4D**). Analysis of cellular composition across samples showed that epithelial cells made up the largest fraction in most samples (**Figure 4E**). To validate this finding, the cell-type-specific expression of CCT5 was further evaluated in an independent dataset (GSE145137), which confirmed higher CCT5 expression in cancer cells (**Figure 4F**). Epithelial clusters were categorized into CCT5-high and CCT5-low states based on cluster-level CCT5 expression (post-clustering annotation; **Figure 4B**). InferCNV analysis revealed that the CCT5-high epithelial subgroup exhibited significantly elevated CNV scores compared to the CCT5-low subgroup, with CNV inferred using epithelial cells as observations and T cells as the reference population. This suggests a higher inferred CNV burden in the CCT5-high group (**Figure 5A**, **5B**). Enrichment analysis indicated that genes upregulated in the CCT5-high subpopulation were associated with cancer-related programs, such as MYC and E2F target gene sets, as well as metabolic pathways related to oxidative phosphorylation (**Figure 5C**). Furthermore, spatial transcriptomics demonstrated the presence of CCT5 expression across various tumor regions (**Figure 5D**). Cell-cell communication analysis showed that CCT5-high epithelial cells exhibited broad interactions with multiple cell populations, including immune cells and fibroblasts, with increased interaction number and strength in the inferred communication network (**Figure 5E**). These results suggest that higher CCT5 expression is associated with a subset of epithelial cells exhibiting distinct CNV features and microenvironmental interaction patterns in BLCA.

CCT5 expression is associated with immune infiltration and checkpoint genes

Given the enrichment of CCT5 in epithelial tumor cells, its potential link with tumor immune modulation was further explored using TCGA data. High CCT5 expression correlated with altered infiltration levels of multiple immune cell subsets, including macrophages, NK cells, and T-cell populations. Moreover, CCT5 was positively associated with several inhibitory and co-stimulatory checkpoint molecules. Detailed results are provided in Figure S2A-E.

Knockdown of CCT5 restrains bladder cancer cell proliferation, invasion, and migration

To investigate the role of CCT5 in the malignant phenotype of BLCA, CCT5 was knocked down in UMUC-3 and T24 cells, which exhibit relatively high expression levels, and stable knockdown cell lines were established. The efficiency of CCT5 knockdown was confirmed through RT-qPCR and Western blotting (**Figure 6A-D**). Cell proliferation was significantly redu-

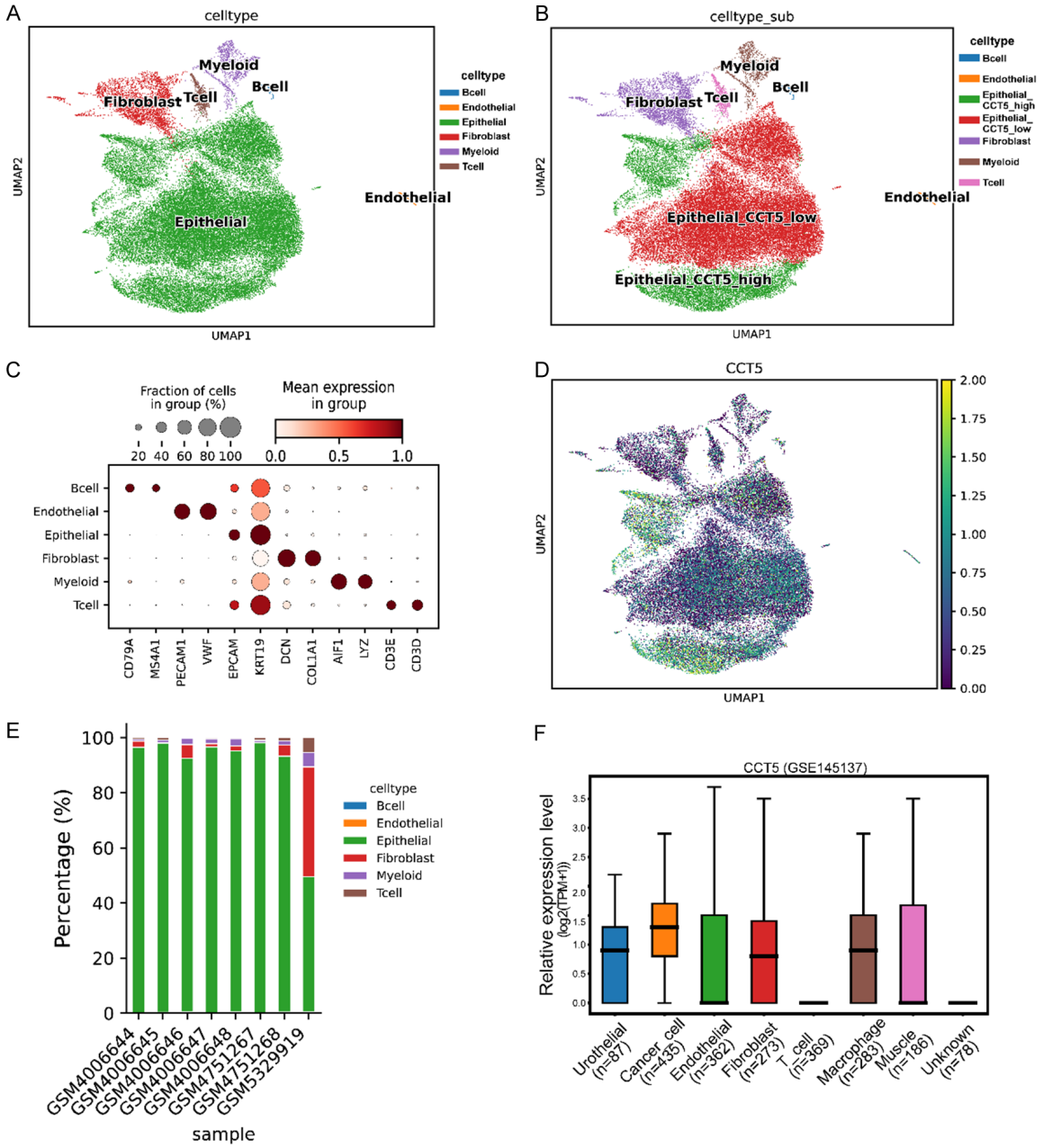

Figure 4. Cell-type distribution of CCT5 at the single-cell level and external validation. A, B. UMAP plot of major cell populations. C. Dot plot of canonical marker genes for cell annotation. D. CCT5 enrichment in epithelial cells. E. Stacked bar plot showing cell-type composition across samples. F. CCT5 expression across cell clusters.

ced in CCT5 knockdown cells (Sh1, Sh2) compared to the negative control (NC) group, as demonstrated by CCK-8 assays (**Figure 6E**, **6F**). Colony formation assays further showed that silencing CCT5 significantly impaired the clonogenic capacity of BLCA cells (**Figure 6G**). Additionally, transwell assays revealed a substantial reduction in both invasion and migration abilities of UMUC-3 and T24 cells following CCT5 knockdown (**Figure 6H**, **6I**). Consistently, wound-healing assays demonstrated a marked suppression of the migratory capacity of UMUC-3 and T24 cells upon CCT5 knockdown (**Figure 6J**, **6K**).

Knockdown of CCT5 results in enhanced apoptotic activity and cell cycle inhibition

Apoptosis analysis by flow cytometry revealed a significant increase in apoptotic rates in CCT5

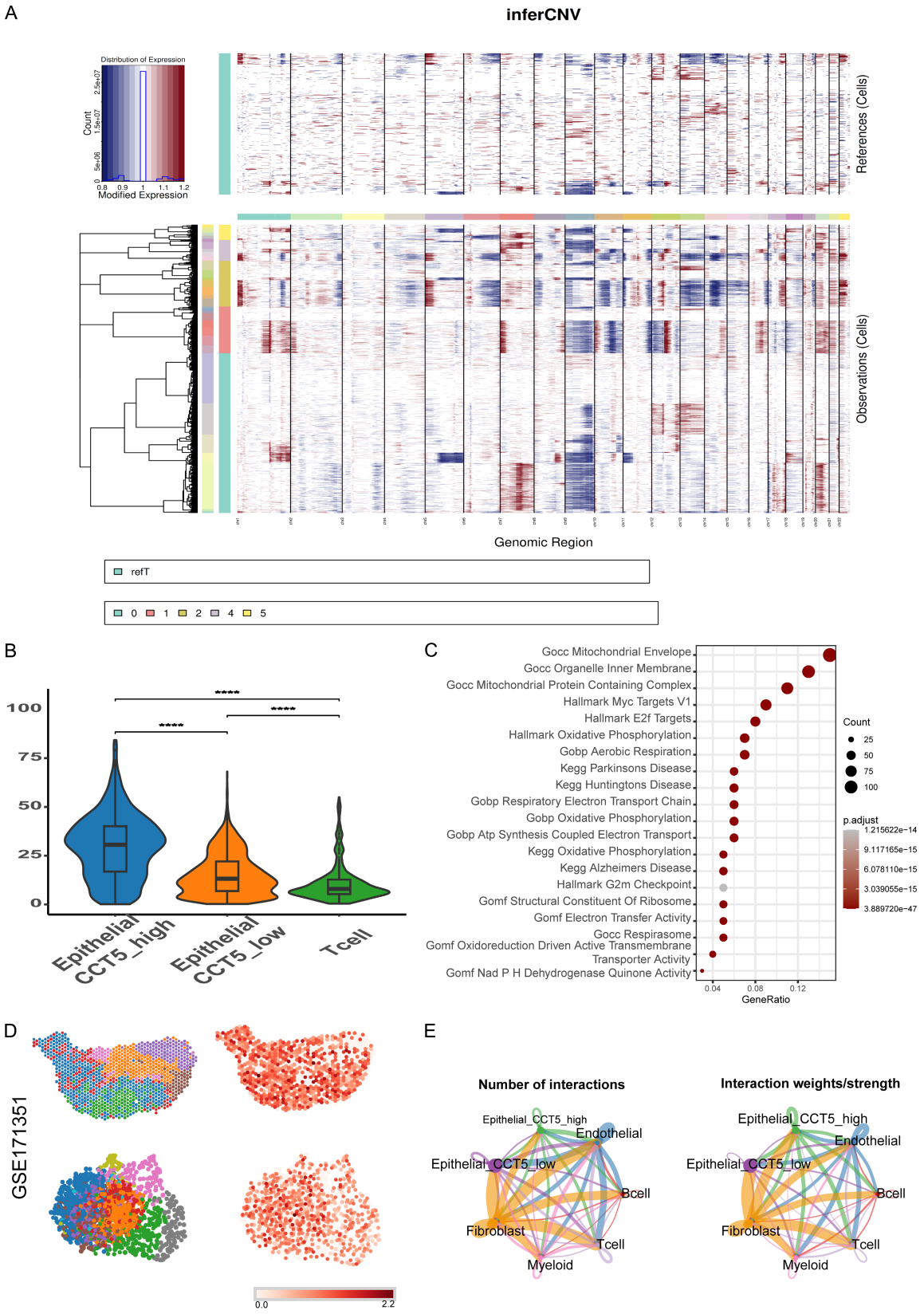

Figure 5. Inferred CNV features and functional associations of CCT5 based on single-cell data. A, B. InferCNV and violin plot showing higher CNV in CCT5-high cells. C. Pathway enrichment of DEGs from CCT5-high epithelial cells. D. Spatial transcriptomics showing CCT5 distribution in tumor areas. E. Cell communication between CCT5-high epithelial and other cell types.

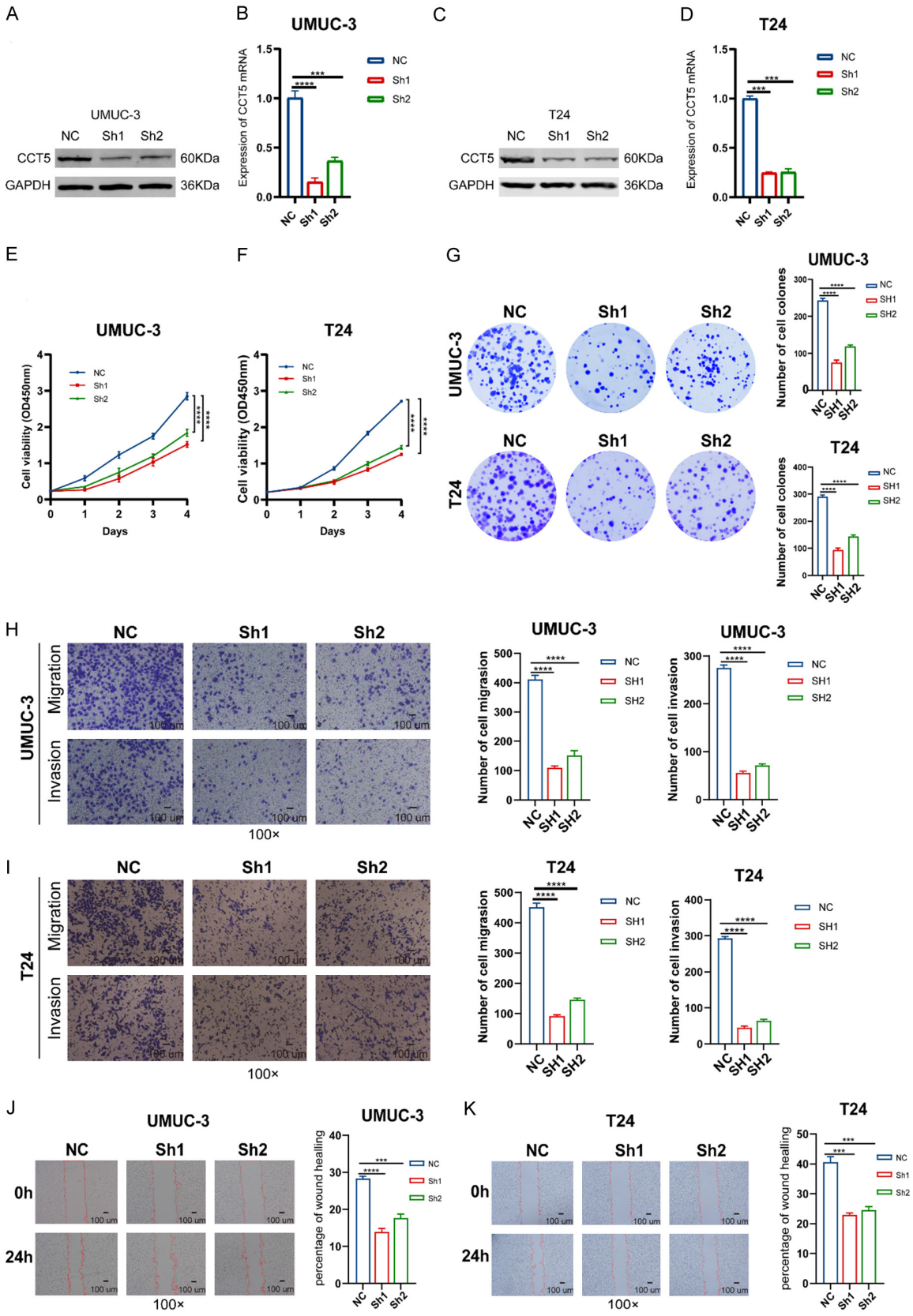

Figure 6. Effects of CCT5 knockdown on malignant phenotypes. A-D. Efficient knockdown of CCT5 in UMUC-3 and T24 cells was validated by Western blot and RT-qPCR. E, F. Proliferation capacity was compromised in CCT5-depleted

cells (shCCT5 groups) as determined by CCK-8 assay. G. Clonogenic survival was markedly attenuated upon CCT5 knockdown, evidenced by a reduction in colony numbers. H, I. Transwell assays revealed impaired migratory and invasive capabilities in CCT5-silenced cells. J, K. Wound healing progression was delayed following CCT5 ablation, indicating suppressed migration.

knockdown UMUC-3 and T24 cells compared to the NC group (**Figure 7A**, **7B**). Cell cycle analysis indicated that CCT5 knockdown led to an increase in the proportion of cells in the G1 phase, accompanied by a reduction in the S and G2 phases, suggesting a G1/S phase arrest (**Figure 7C**, **7D**). Western blotting confirmed these findings, showing a marked decrease in the expression of key cell cycle regulators (Cyclin D1, CDK4, CDK6) in the CCT5 knockdown groups compared to the NC group (**Figure 7E**, **7F**).

CCT5 overexpression drives malignant progression

To validate the oncogenic role of CCT5, a stable CCT5-overexpressing J82 cell line was generated, with successful overexpression verified by RT-qPCR and Western blotting (**Figure 8A**, **8B**). Functional assays demonstrated that ectopic CCT5 expression significantly enhanced cellular growth and clonogenicity (**Figure 8C**, **8D**). Furthermore, invasion, migration, and wound-healing capacities were notably increased in CCT5-overexpressing cells compared to the vector control group (**Figure 8E**, **8F**). Flow cytometric apoptosis assays showed that CCT5 overexpression significantly suppressed apoptotic rates relative to the vector control group (**Figure 8G**). Cell cycle analysis by flow cytometry revealed that forced expression of CCT5 accelerated the G1/S transition, as evidenced by a reduction in the proportion of G1-phase cells and a simultaneous increase in the S and G2-phase populations. Western blotting analysis confirmed increased expression of Cyclin D1, CDK4, and CDK6 in CCT5-overexpressing cells compared to the vector control group (**Figure 8H**, **8I**).

CCT5 knockdown attenuates subcutaneous tumor growth in nude mice

Subcutaneous xenograft tumors were generated by injecting UMUC-3 cells with stable CCT5 knockdown or NC group cells into mice. Tumor growth was monitored over time, and CCT5 depletion significantly delayed tumor progression, resulting in smaller tumor volumes and lower weights compared to controls (**Figure 9A-C**). Consistent with these findings, IHC showed reduced Ki67 expression in tumors derived from CCT5-knockdown cells (**Figure 9D**).

CCT5 drives bladder cancer progression via modulation of the Hippo/YAP pathway

To investigate the underlying molecular mechanisms, RNA-seq analysis was performed on T24 cells following CCT5 depletion. Volcano plot and heatmap analyses revealed that several downstream targets of the Hippo pathway, including BMP4, CCN1, AMOT, and CCN2, were significantly downregulated after CCT5 knockdown (**Figure 9E**, **9F**). Functional enrichment analysis of the differentially expressed genes suggested involvement in processes such as wound healing, cell development, and growth factor activity, with KEGG analysis highlighting significant enrichment in the Hippo signaling pathway (**Figure 9G**, **9H**). Western blotting analysis revealed that CCT5 knockdown promoted phosphorylation of MST1, LATS1, and YAP1, while their total protein expression remained unchanged (**Figure 9I**, **9J**). This pattern indicates activation of the Hippo cascade and inhibition of YAP-driven transcription. These results suggest that CCT5 promotes BLCA progression through modulation of the Hippo signaling pathway.

Discussion

This study demonstrates that CCT5 is significantly upregulated in BLCA at both the transcriptional and protein levels. Elevated CCT5 expression is strongly associated with poor survival outcomes and aggressive pathological features. Functional experiments, both *in vitro* and *in vivo*, further confirm that CCT5 enhances the malignant behavior of BLCA cells. Mechanistically, our data suggest that CCT5 regulates the Hippo/YAP axis: CCT5 knockdown increases phosphorylation of MST1, LATS1, and YAP, while the total protein levels of these molecules remain unchanged. In conclusion, this study provides evidence that CCT5 promotes BLCA progression and may serve as both a clinical biomarker and a therapeutic target.

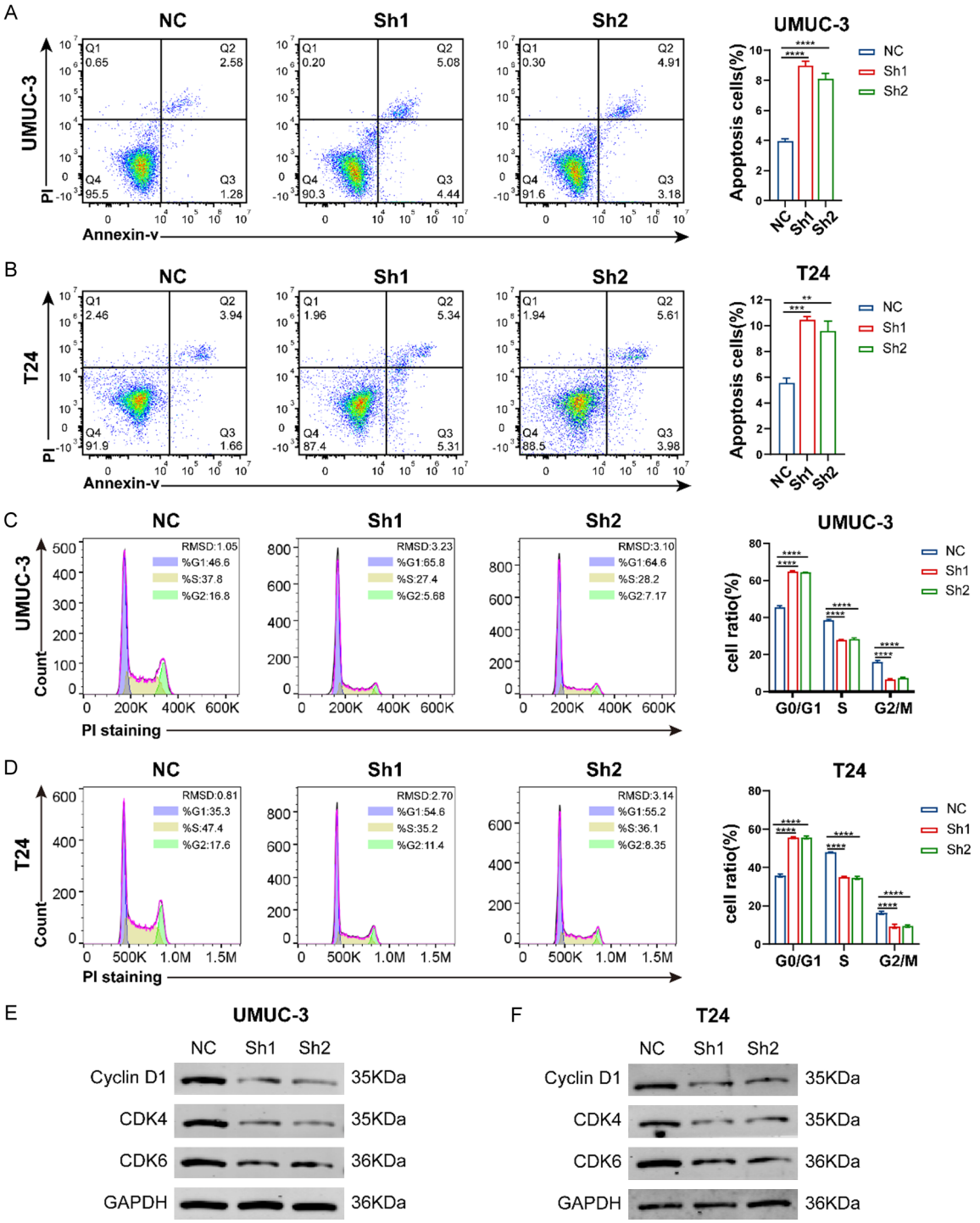

Figure 7. Knockdown of CCT5 results in enhanced apoptotic activity and cell cycle inhibition. A, B. Flow cytometric analysis revealed a significant increase in apoptosis upon CCT5 knockdown in UMUC-3 and T24 cells. C, D. CCT5 depletion induced cell cycle arrest at the G1 phase, accompanied by a reduction in S and G2/M phase populations. E, F. Western blotting confirmed concomitant downregulation of key G1/S checkpoint regulators (Cyclin D1, CDK4, CDK6) in CCT5-deficient cells.

Notably, our single-cell and spatial transcriptomic analyses offer additional validation and mechanistic insight into the role of CCT5 in BLCA. CCT5 expression is predominantly enriched in epithelial tumor cells, with a distinct CCT5-high subpopulation exhibiting higher CNV

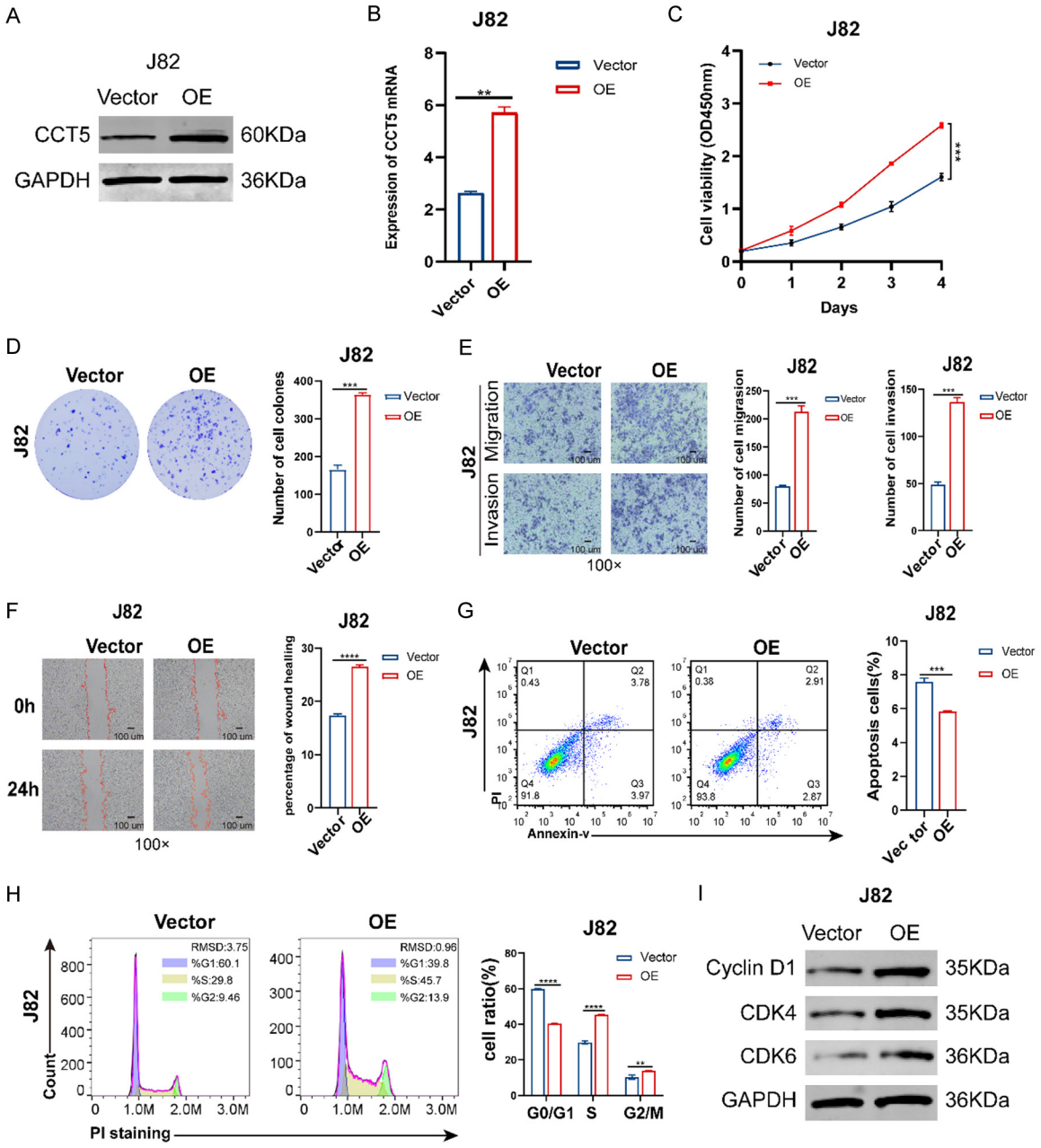

Figure 8. CCT5 overexpression drives malignant progression. A, B. Overexpression of CCT5 in J82 cells was confirmed by RT-qPCR and Western blot. C, D. Enhanced proliferative and clonogenic capacity was observed upon CCT5 overexpression, as assessed by CCK-8 and colony formation assays. E, F. Migration, invasion, and wound healing assays demonstrated promoted migratory ability in CCT5-overexpressing cells. G. Flow cytometry indicated that CCT5 overexpression attenuated apoptosis. H, I. Cell cycle analysis and Western blot revealed that CCT5 overexpression accelerated G1/S transition and upregulated expression of Cyclin D1, CDK4, and CDK6.

scores and enrichment of oncogenic MYC and E2F target programs. Spatial transcriptomics further confirmed the widespread expression of CCT5 in tumor tissues, while intercellular communication analysis revealed extensive interactions between CCT5-high epithelial cells and immune and stromal populations. These findings highlight CCT5 as a marker of malignant epithelial subsets and suggest its potential role in influencing the tumor microenvironment through epithelial-immune crosstalk.

Enrichment analyses based on the TCGA cohort highlight cell cycle-related processes, while transcriptomic profiling of T24 cells after CCT5 knockdown reveals enrichment in developmen-

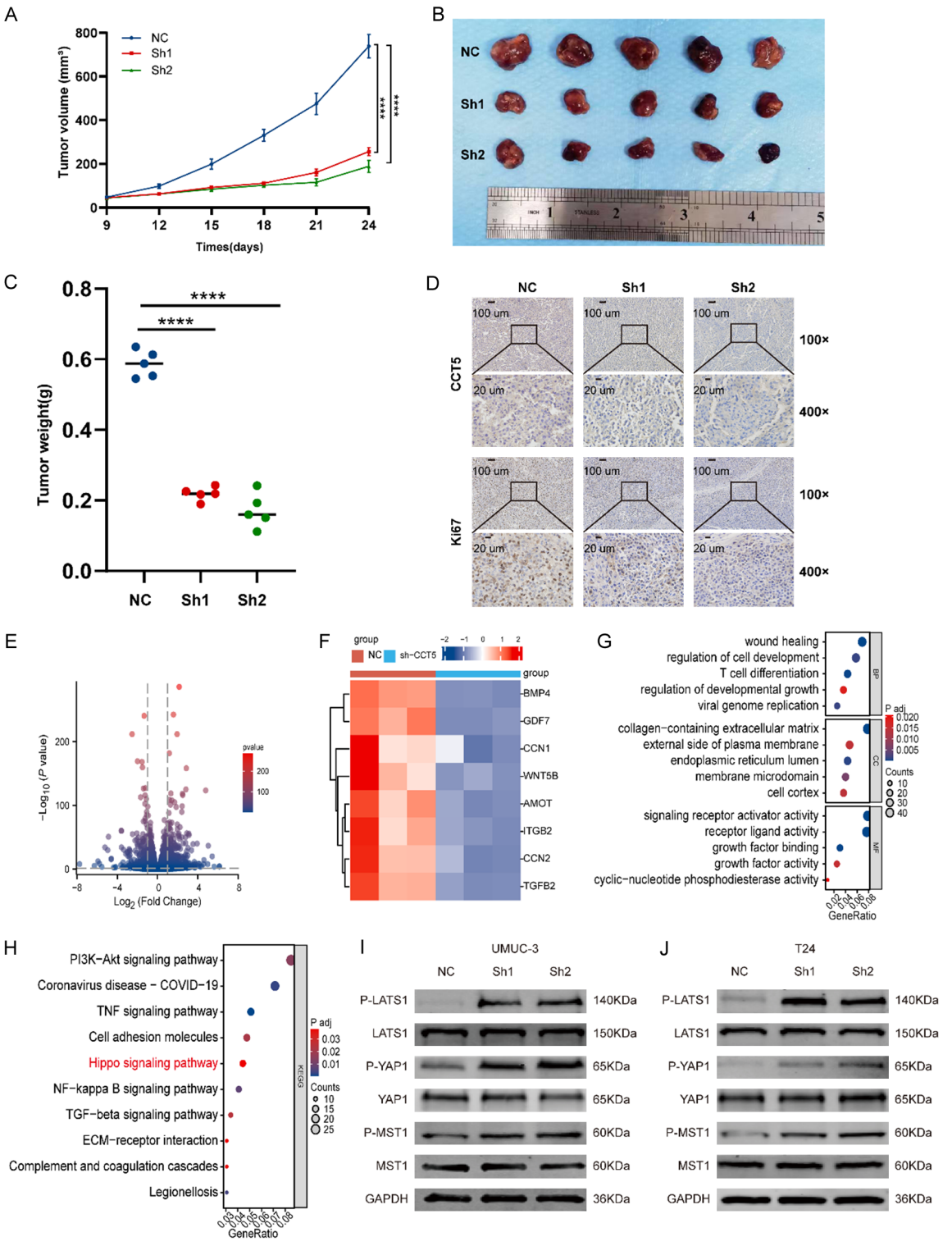

Figure 9. CCT5 knockdown suppresses tumor growth in vivo and activates Hippo signaling. A-C. Subcutaneous xenograft models demonstrated impaired tumor growth upon CCT5 knockdown. D. Tumors with CCT5 knockdown exhibited lower proliferative index, as indicated by reduced Ki-67 staining. E, F. Transcriptomic profiling revealed downregulation of Hippo pathway downstream effectors (e.g., BMP4, CCN1, AMOT, CCN2). G, H. GO and KEGG analyses of differentially expressed genes highlighted enrichments in processes including wound healing, cell development, and Hippo signaling. I, J. Western blot analysis confirmed activation of the Hippo pathway, evidenced by enhanced phosphorylation of MST1, LATS1, and YAP without alterations in total protein levels.

tal and wound-healing pathways. Our single-cell data complement these findings, demonstrating that CCT5-high epithelial cells are enriched in proliferative and malignant signaling, consistent with the oncogenic roles observed in bulk RNA-seq and functional assays. Together, these results indicate that CCT5 contributes to BLCA progression by driving intrinsic proliferative programs and shaping extrinsic cellular interactions.

Our observations align with previous studies showing that CCT5 promotes malignant phenotypes in other cancers. In lung adenocarcinoma, CCT5 enhances invasion and migration through interactions with cyclin D1 and activation of the PI3K/AKT pathway [15]. In gastric cancer, CCT5 upregulation is linked to aggressive phenotypes, including epithelial-mesenchymal transition (EMT) and lymph node metastasis, through activation of the Wnt/β-catenin pathway [17]. Research on hepatocellular carcinoma has shown that CCT5 facilitates progression by accelerating cell cycle transition and increasing invasive potential [16]. These findings highlight CCT5's role in promoting malignant progression across various cancers, suggesting that its chaperonin function is coupled with oncogenic signaling pathways.

The Hippo/YAP association identified in this study is biologically plausible within the context of BLCA. Aberrations in the Hippo pathway are critically involved in urothelial carcinoma pathogenesis, promoting proliferation, apoptosis evasion, and the acquisition of EMT, with YAP/TAZ acting as key nuclear transcriptional effectors of this pathway [29, 30]. Our findings demonstrate that CCT5 knockdown increases the phosphorylation of MST1, LATS1, and YAP, supporting a model in which CCT5 inhibits Hippo signaling to maintain YAP activity. Loss of CCT5, conversely, restores Hippo pathway activation and reduces YAP transcriptional function. Whether CCT5 exerts this effect indirectly through chaperoning cytoskeletal components or directly *via* interactions with core pathway factors requires further investigation.

Beyond the Hippo pathway, independent evidence suggests that CCT5 intersects with multiple oncogenic signaling networks. In head and neck cancer models, CCT5 functions downstream of the β-catenin/CBP-mTORC1 axis to regulate EMT-related gene programs [14]. In colorectal cancer, CCT5 interacts with asparagine synthetase (ASNS) to promote asparagine biosynthesis, thereby activating mTORC1 signaling and enhancing tumor proliferation and immunosuppression; this effect can be reversed by asparaginase, which synergizes with anti-PD-L1 therapy [13]. These studies, despite tissue-specific variations, highlight a broader paradigm in which CCT5 links protein homeostasis to metabolic and transcriptional drivers, facilitating malignant progression. This mechanism warrants further exploration in BLCA.

While bulk RNA-seq analysis suggested a potential link between CCT5 and tumor immune infiltration, our single-cell results revealed that CCT5 expression is predominantly confined to epithelial tumor cells. This implies that the immunological associations observed in bulk analyses may be mediated indirectly through epithelial-immune interactions, rather than direct expression in immune cells. Thus, although CCT5 may contribute to shaping an immunosuppressive tumor microenvironment, additional functional studies are required to clarify the exact mechanisms.

At the functional level, our gain- and loss-of-function experiments demonstrated that CCT5 promotes cell growth, clonogenic potential, motility, and invasiveness. Conversely, CCT5 downregulation induced apoptosis and G1/S arrest, accompanied by reduced expression of Cyclin D1, CDK4, and CDK6. These *in vitro* findings were corroborated *in vivo*, where CCT5 knockdown inhibited xenograft tumor growth and decreased Ki-67 expression. Our results align with previous studies showing that the TRiC/CCT complex supports cell cycle progression and inhibits apoptotic pathways [16, 31, 32], reinforcing the potential of CCT5 as a therapeutic target.

From a translational perspective, this study carries several important implications. First, CCT5 may have diagnostic value: our ROC analysis (AUC ≈ 0.84) demonstrated good performance in distinguishing tumor from normal tissues, suggesting that CCT5 could complement cystoscopy and molecular testing. Second, single-cell and spatial transcriptomics enabled us to identify CCT5-high malignant epithelial subsets, which may provide a foundation for developing precision therapies targeting specific cellular populations. Although no direct CCT5 inhibitors are currently available, ongoing structural and functional studies of the TRiC/CCT

complex could lead to strategies that disrupt CCT5-client interactions or inhibit its chaperonin activity. Finally, given that Hippo/YAP signaling is associated with immune escape and that pan-cancer studies link CCT5 to an immunosuppressive tumor microenvironment, it is crucial to investigate whether CCT5 influences immune infiltration and checkpoint regulation in BLCA.

However, this study has several limitations. First, transcriptomic analyses can only suggest correlations, not causality. While our intervention experiments support the proposed mechanistic model, it remains unclear whether CCT5 regulates the Hippo pathway through direct or indirect mechanisms. Further studies, such as MST1/2 inhibition rescue assays, ChIP-qPCR, and proteomic interaction profiling, will be needed to clarify this mechanism. Second, our animal experiments relied on subcutaneous xenografts, a model that does not fully reflect the complexity of the natural tumor microenvironment. Third, the single-cell dataset analyzed here had a limited sample size, and additional validation in larger independent cohorts is necessary. Future research should also focus on developing pharmacological tools targeting the CCT5/TRiC complex - especially strategies aimed at disrupting specific client-CCT5 interactions - to assess the clinical feasibility of targeting CCT5.

In conclusion, this study highlights CCT5 as an oncogenic factor in BLCA. CCT5 is significantly upregulated and associated with aggressive clinicopathological features and poor survival. Experimental evidence confirms that CCT5 promotes malignant phenotypes, such as increased BLCA cell proliferation, and suggests that its pro-tumor effects may be mediated by modulating the Hippo/YAP signaling pathway. These findings position CCT5 as a potential prognostic marker and an attractive therapeutic target, providing a theoretical foundation for future translational research focused on targeting CCT5 for BLCA treatment.

Disclosure of conflict of interest

None.

Address correspondence to: Panfeng Shang, Department of Urology, Gansu Province Clinical Research Center for Urinary System Disease, The Second Hospital of Lanzhou University, Lanzhou 730030, Gansu, China. E-mail: shangpf@lzu.edu.cn; Yanzong Zhao, Department of Urology, The First Hospital of Lanzhou University, Lanzhou 730000, Gansu, China. E-mail: tsguoxt@163.com

References

[1] Bray F, Laversanne M, Sung H, Ferlay J, Siegel RL, Soerjomataram I and Jemal A. Global cancer statistics 2022: GLOBOCAN estimates of incidence and mortality worldwide for 36 cancers in 185 countries. CA Cancer J Clin 2024; 74: 229-263.

[2] Babjuk M, Burger M, Capoun O, Cohen D, Compérat EM, Dominguez Escrig JL, Gontero P, Liedberg F, Masson-Lecomte A, Mostafid AH, Palou J, van Rhijn BWG, Rouprêt M, Shariat SF, Seisen T, Soukup V and Sylvester RJ. European association of urology guidelines on non-muscle-invasive bladder cancer (Ta, T1, and Carcinoma in Situ). Eur Urol 2022; 81: 75-94.

[3] Mertens LS, Claps F, Mayr R, Bostrom PJ, Shariat SF, Zwarthoff EC, Boormans JL, Abas C, van Leenders GJLH, Götz S, Hippe K, Bertz S, Neuzillet Y, Sanders J, Broeks A, Peters D, van der Heijden MS, Jewett MAS, Stöhr R, Zlotta AR, Eckstein M, Soorojebally Y, van der Schoot DKE, Wullich B, Burger M, Otto W, Radvanyi F, Sirab N, Pouessel D, van der Kwast TH, Hartmann A, Lotan Y, Allory Y, Zuiverloon TCM and van Rhijn BWG. Prognostic markers in invasive bladder cancer: FGFR3 mutation status versus P53 and KI-67 expression: a multi-center, multi-laboratory analysis in 1058 radical cystectomy patients. Urol Oncol 2022; 40: 110.e111-110.e119.

[4] Matuszczak M and Salagierski M. Diagnostic and prognostic potential of biomarkers CYFRA 21.1, ERCC1, p53, FGFR3 and TATI in bladder cancers. Int J Mol Sci 2020; 21: 3360.

[5] Patel VG, Oh WK and Galsky MD. Treatment of muscle-invasive and advanced bladder cancer in 2020. CA Cancer J Clin 2020; 70: 404-423.

[6] Lenis AT, Lec PM, Chamie K and Mshs MD. Bladder cancer: a review. JAMA 2020; 324: 1980-1991.

[7] Antoni S, Ferlay J, Soerjomataram I, Znaor A, Jemal A and Bray F. Bladder cancer incidence and mortality: a global overview and recent trends. Eur Urol 2017; 71: 96-108.

[8] Leitner A, Joachimiak LA, Bracher A, Mönkemeyer L, Walzthoeni T, Chen B, Pechmann S, Holmes S, Cong Y, Ma B, Ludtke S, Chiu W, Hartl FU, Aebersold R and Frydman J. The molecular architecture of the eukaryotic chaperonin TRiC/CCT. Structure 2012; 20: 814-825.

[9] McClellan AJ, Scott MD and Frydman J. Folding and quality control of the VHL tumor suppressor proceed through distinct chaperone pathways. Cell 2005; 121: 739-748.

[10] Llorca O, Martín-Benito J, Ritco-Vonsovici M, Grantham J, Hynes GM, Willison KR, Carrasco-

sa JL and Valpuesta JM. Eukaryotic chaperonin CCT stabilizes actin and tubulin folding intermediates in open quasi-native conformations. EMBO J 2000; 19: 5971-5979.
[11] Kasembeli M, Lau WC, Roh SH, Eckols TK, Frydman J, Chiu W and Tweardy DJ. Modulation of STAT3 folding and function by TRiC/CCT chaperonin. PLoS Biol 2014; 12: e1001844.
[12] Camasses A, Bogdanova A, Shevchenko A and Zachariae W. The CCT chaperonin promotes activation of the anaphase-promoting complex through the generation of functional Cdc20. Mol Cell 2003; 12: 87-100.
[13] Zhang Y, Zhao W, Wu L, Ai T, He J, Chen Z, Wang C, Wang H, Zhou R, Liu C and Zhao L. Inhibition of CCT5-mediated asparagine biosynthesis and anti-PD-L1 produce synergistic antitumor effects in colorectal cancer. Acta Pharm Sin B 2025; 15: 2480-2497.
[14] Reed ER, Jankowski SA, Spinella AJ, Noonan V, Haddad R, Nomoto K, Matsui J, Bais MV, Varelas X, Kukuruzinska MA and Monti S. β-catenin/CBP activation of mTORC1 signaling promotes partial epithelial-mesenchymal states in head and neck cancer. Transl Res 2023; 260: 46-60.
[15] Meng Y, Yang L, Wei X, Luo H, Hu Y, Tao X, He J, Zheng X, Xu Q, Luo K, Yu G and Luo Q. CCT5 interacts with cyclin D1 promoting lung adenocarcinoma cell migration and invasion. Biochem Biophys Res Commun 2021; 567: 222-229.
[16] Liu J, Huang L, Zhu Y, He Y, Zhang W, Lei T, Xuan J, Xiao B, Li L, Zhou Q and Sun Z. Exploring the expression and prognostic value of the TCP1 ring complex in hepatocellular carcinoma and overexpressing its subunit 5 promotes HCC tumorigenesis. Front Oncol 2021; 11: 739660.
[17] Li Y, Liu C, Zhang X, Huang X, Liang S, Xing F and Tian H. CCT5 induces epithelial-mesenchymal transition to promote gastric cancer lymph node metastasis by activating the Wnt/β-catenin signalling pathway. Br J Cancer 2022; 126: 1684-1694.
[18] He J, McLaughlin RP, van der Beek L, Canisius S, Wessels L, Smid M, Martens JWM, Foekens JA, Zhang Y and van de Water B. Integrative analysis of genomic amplification-dependent expression and loss-of-function screen identifies ASAP1 as a driver gene in triple-negative breast cancer progression. Oncogene 2020; 39: 4118-4131.
[19] Wu S and Peng L. Increased CCT5 expression is a potential unfavourable factor promoting the growth of nasopharyngeal carcinoma. J Int Med Res 2024; 52: 3000605241271754.
[20] Ooe A, Kato K and Noguchi S. Possible involvement of CCT5, RGS3, and YKT6 genes up-regulated in p53-mutated tumors in resistance to docetaxel in human breast cancers. Breast Cancer Res Treat 2007; 101: 305-315.
[21] Dey A, Varelas X and Guan KL. Targeting the Hippo pathway in cancer, fibrosis, wound healing and regenerative medicine. Nat Rev Drug Discov 2020; 19: 480-494.
[22] Ma S, Meng Z, Chen R and Guan KL. The Hippo pathway: biology and pathophysiology. Annu Rev Biochem 2019; 88: 577-604.
[23] Yu FX, Zhao B and Guan KL. Hippo pathway in organ size control, tissue homeostasis, and cancer. Cell 2015; 163: 811-828.
[24] Fu M, Hu Y, Lan T, Guan KL, Luo T and Luo M. The Hippo signalling pathway and its implications in human health and diseases. Signal Transduct Target Ther 2022; 7: 376.
[25] Xie B, Lin J, Chen X, Zhou X, Zhang Y, Fan M, Xiang J, He N, Hu Z and Wang F. CircXRN2 suppresses tumor progression driven by histone lactylation through activating the Hippo pathway in human bladder cancer. Mol Cancer 2023; 22: 151.
[26] Sadhukhan P, Feng M, Illingworth E, Sloma I, Ooki A, Matoso A, Sidransky D, Johnson BA 3rd, Marchionni L, Sillé FC, Choi W, McConkey D and Hoque MO. YAP1 induces bladder cancer progression and promotes immune evasion through IL-6/STAT3 pathway and CXCL deregulation. J Clin Invest 2024; 135: e171164.
[27] Livak KJ and Schmittgen TD. Analysis of relative gene expression data using real-time quantitative PCR and the 2(-Delta Delta C(T)) method. Methods 2001; 25: 402-408.
[28] Rong L, Li Z, Leng X, Li H, Ma Y, Chen Y and Song F. Salidroside induces apoptosis and protective autophagy in human gastric cancer AGS cells through the PI3K/Akt/mTOR pathway. Biomed Pharmacother 2020; 122: 109726.
[29] Xia J, Zeng M, Zhu H, Chen X, Weng Z and Li S. Emerging role of Hippo signalling pathway in bladder cancer. J Cell Mol Med 2018; 22: 4-15.
[30] Liu JY, Li YH, Lin HX, Liao YJ, Mai SJ, Liu ZW, Zhang ZL, Jiang LJ, Zhang JX, Kung HF, Zeng YX, Zhou FJ and Xie D. Overexpression of YAP 1 contributes to progressive features and poor prognosis of human urothelial carcinoma of the bladder. BMC Cancer 2013; 13: 349.
[31] Zeng G, Wang J, Huang Y, Lian Y, Chen D, Wei H, Lin C and Huang Y. Overexpressing CCT6A contributes to cancer cell growth by affecting the G1-To-S phase transition and predicts a negative prognosis in hepatocellular carcinoma. Onco Targets Ther 2019; 12: 10427-10439.
[32] Won KA, Schumacher RJ, Farr GW, Horwich AL and Reed SI. Maturation of human cyclin E requires the function of eukaryotic chaperonin CCT. Mol Cell Biol 1998; 18: 7584-7589.

Table S1. Primer sequences used for qRT-PCR analysis

Gene	Direction	Sequence (5'→3')
CCT5	Forward	CATAAGCTGGATGTGACCTCT
	Reverse	GCCCCACTGACAAATTGCTA
β-actin	Forward	GAGCACAGAGCCTCGCCTTT
	Reverse	ACATGCCGGAGCCGTTGTC

Table S2. Sequences of shRNAs used for knockdown in stable cell lines

Name	Forward Primer
shRNA1	GATCCGGCATTCACCCAATCAGAATACTCGAGTATTCTGATTGGGTGAATGCCTTTTTTG
shRNA2	GATCCGATAGCGTCCTTGTTGACATAACTCGAGTTATGTCAACAAGGACGCTATTTTTTTG
NC	GATCCGTTCTCCGAACGTGTCACGTAATTCAAGAGATTACGTGACACGTTCGGAGAATTTTTTC

Note: NC, non-targeting negative control.

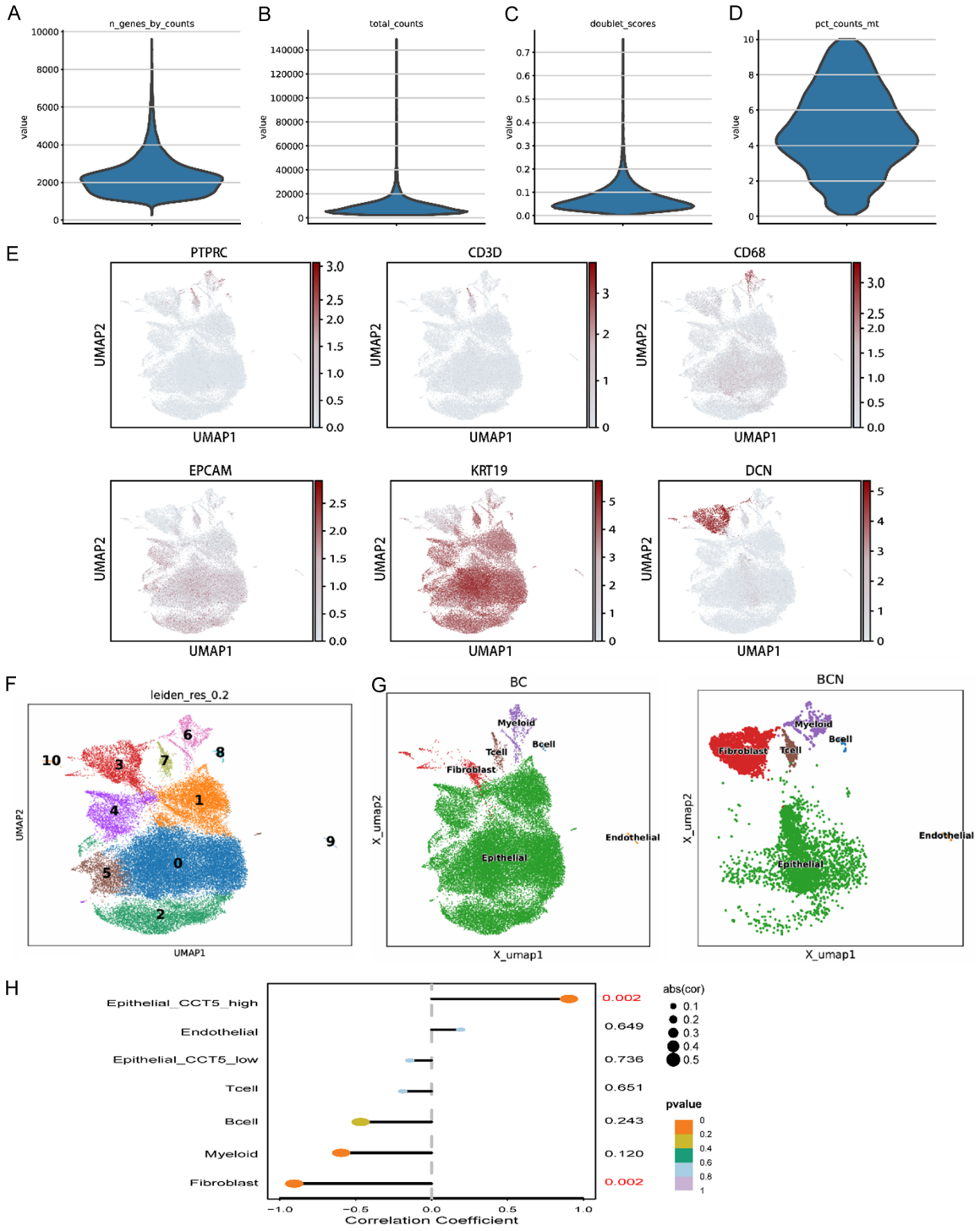

Figure S1. Quality control and cell-type annotation of single-cell RNA-seq data from the GSE135337 cohort. (A-D) Quality control (QC) metrics applied to single-cell data prior to analysis, encompassing the number of detected genes (A), total UMI counts (B), doublet scores (C), and mitochondrial transcript percentage (D). Cells failing QC thresholds were filtered out. (E) Cell type identity was assigned based on expression of established marker genes: PTPRC (immune cells), CD3D (T cells), CD68 (myeloid cells), DCN (fibroblasts), and KRT19/EPCAM (epithelial cells), visualized on UMAP plots. (F) Unsupervised clustering of cells revealed 11 distinct populations (0-10). (G) Compositional analysis showed enrichment of epithelial cells in tumor samples (BC) compared to matched adjacent normal tissue (BCN). (H) CCT5-high epithelial subpopulations were correlated with malignant tumor characteristics.

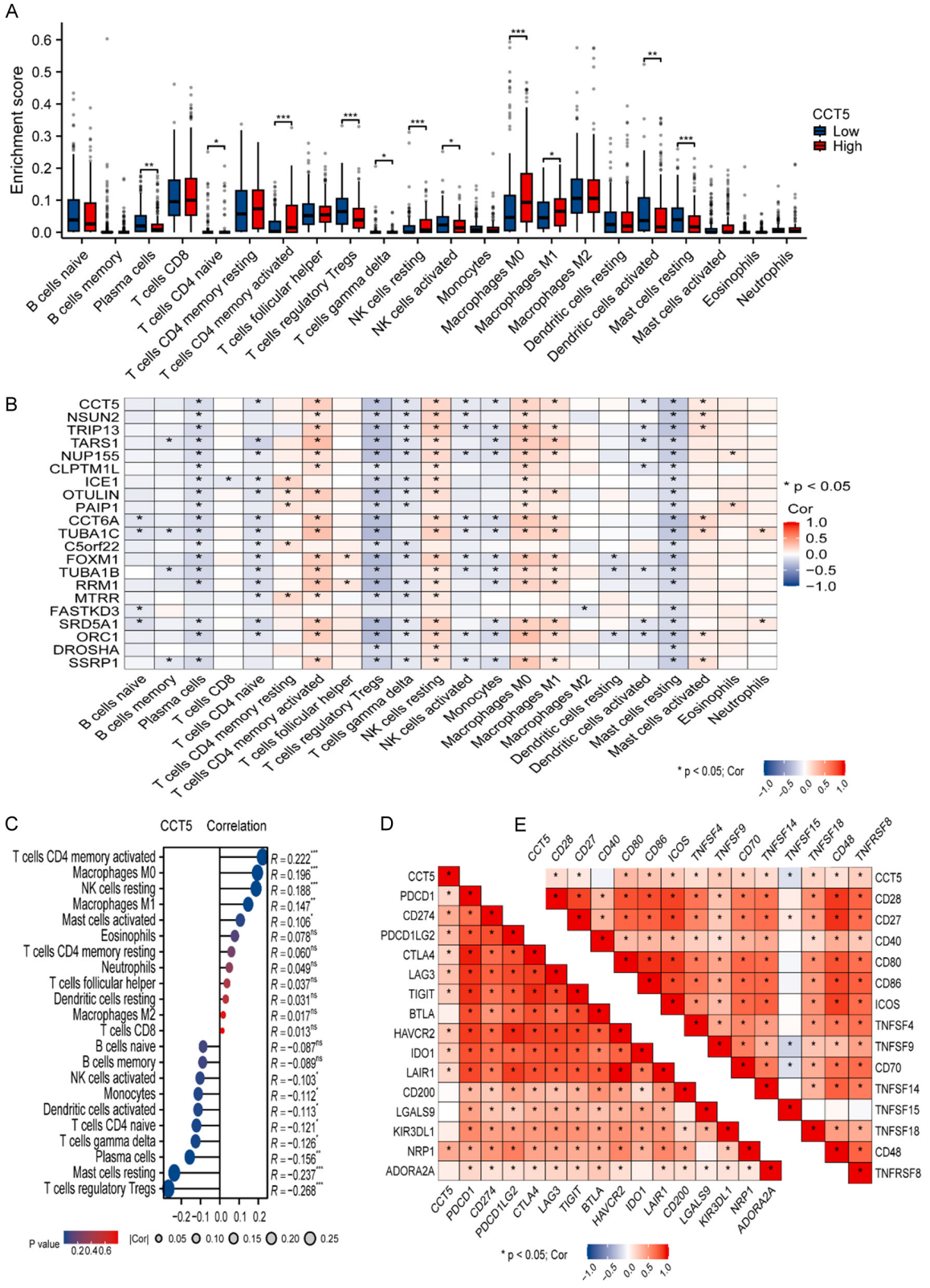

Figure S2. Association of CCT5 expression with immune infiltration profiles and immune checkpoint molecules. (A) Comparative analysis of immune cell infiltration between tumors with high and low CCT5 expression. (B) Correlation heatmap of CCT5 and its co-expressed genes with various immune cell subsets. (C) CCT5 expression levels showed significant correlations with the abundance of specific immune cells, including M0/M2 macrophages, activated memory CD4+ T cells, resting NK cells, and regulatory T cells (Tregs). (D, E) Scatter plots depicting the relationship between CCT5 expression and the transcript levels of inhibitory (D) and stimulatory (E) immune checkpoint molecules.